MEASURING SURFACE TEMPERATURES OF DIFFERENT TYPES OF FLY ASH SAMPLES USING A CCD CAMERA

by

Huawei LIU[a], Runru ZHU[b*], Xin WANG[c], Gengda LI[c], Qingru CUI[c], Chao XU[a], and Yun HUANG[b]

[a] Key Laboratory of Condition Monitoring and Control for Power Equipment, Ministry of Education of China, School of Energy, Power and Mechanical Engineering, North China Electric Power University, Changping District, Beijing, China
[b] State Key Laboratory of Multiphase Complex Systems, Institute of Process Engineering, Chinese Academy of Sciences, Haidian District Beijing, China
[c] Guodian New Energy Technology Research Institute Co., Ltd, Changping District, Beijing, China

Original scientific paper
https://doi.org/10.2298/TSCI200620191L

In this work, an optical emission-based two-color method was experimentally investigated for the measurement of surface temperatures of different types of fly ash samples using a CCD camera. A heating system consisting of a Hencken flat-flame burner, a narrow piece of stainless steel wire mesh to separate the flame and the ash samples to be studied, and a thermocouple to record the temperature, was used to heat fly ash samples. A color camera equipped with a tri-band filter was used to capture radiation images. Fly ash samples collected from three kinds of coal-fired boilers were heated and imaged at different temperatures. The chemical compositions, elements, and particle size distributions were analyzed. The emissivity ratios of the wavelengths corresponding to the R and G optical channels and permitted by the tri-band filter were experimentally determined. A two-color method was subsequently used to calculate the average surface temperatures with relative errors within ±2% in the experiments, and an uncertainty analysis was conducted. Surface temperature distributions were also calculated and presented. The results demonstrate that the emission-based two-color method can be used to determine reliable average surface temperatures and surface temperature distributions when the radiation emitted from the ash samples is obviously greater than the ambient light. The results also show that the method has a lower limit of temperature measurement, which will lessen with the use of larger apertures and a higher radiation capacity of the ash samples to be studied.

Key words: *fly ash, surface temperature, emissivity, two-color method*

Introduction

Surfaces of boiler tubes often suffer from serious ash deposition due to long exposure to high-temperature and dusty flue gas environments. Ash deposits on the convection surfaces can decrease thermal efficiency, and can even cause boiler tube failures [1-4].

Ash deposition is a dynamic process, and the ash-blowing parameters therefore depend greatly on the real-time monitoring of the ash deposition status. Directly visible morphological features can be used to describe the status of the ash deposition, and these features can

* Corresponding author, e-mail: rrzhu@ipe.ac.cn

be monitored using imaging devices, however, protecting camera lenses from high temperatures and dust remains a key problem. Zhou *et al.* [5, 6] used a digital imaging system protected by cooling water and compressed air to monitor the growth of ash deposition. Additionally, surface temperature plays an important role in ash deposition [7-10]. Zhou *et al.* [11] found that the temperature of the deposition surface had a significant effect on the deposition rate and morphology, and that the deposition thickness increased as the surface temperature decreased. Ash deposits also provide thermal resistance, and the surface temperatures of ash deposits increase with growth [12]. Zhou *et al.* [6] also calculated the effective thermal conductivity, which is a key parameter in ash deposition modeling and boiler design. In the calculations, the surface temperature was measured by thermocouples using a method developed by Zheng *et al.* [13]. A thermocouple provides the temperature of a single point, however, the temperatures of a surface may not be consistent. Panchal *et al.* [14] used ten thermocouples to record the surface temperatures of a battery, under the assumption that each temperature represented an average temperature of the area around the sensor. Thermocouples have small dimensions and ease of handling but are required to be attached to the surfaces that they measure [15, 16], for example, Martinez *et al.* [17] welded 26 thermocouples directly into a wall plate to measure wall temperatures. Moreover, the use of thermocouples affects the nearby flow field [18].

The optical emission-based method is sometimes used for the measurement of the temperature of power utility boilers and furnaces, due to its non-invasiveness, minimal disturbance, and ease of acquiring the temperature distribution [19-23]. Based on color images captured with color cameras, temperature distributions can be determined according to the radiation intensity captured by the optical channels. For calculation, the two-color method, which eliminates the influence of all other factors except the temperature, is widely used [24-27]. Huang *et al.* [28] used an RGB pyrometer to measure the surface temperature of a deposit. Via the RGB pyrometer [25, 28, 29], temperatures are calculated according to the response ratios of the optical channels, which is called color-ratio pyrometry, and the grey-body assumption is adopted. In color-ratio pyrometry, the temperature is determined based on the relationship between the response ratio and the temperature, while the differences in the radiation characteristics are ignored, *i.e.*, the grey-body assumption is adopted. With the intensity-ratio method, temperatures are calculated according to the ratios of intensity with assumed or pre-determined radiative characteristics, and the adoption of the grey-body assumption can therefore be avoided. The use of filters to let narrow-bandwidth emissions pass through each optical channel further increases the measurement accuracy [30, 31]. However, little research has focused on the surface temperature measurement of ash depositions using the intensity-ratio method. Therefore, this paper focuses on the experimental investigation of the radiative characteristics of different types of fly ash samples necessary for the implementation of the intensity-ratio method, and the experimental verification of the feasibility of the method for the measurement of the surface temperatures of fly ash samples.

In this paper, the surface temperatures of three types of fly ash samples are experimentally investigated using an optical emission-based method. First, the experimental set-up is briefly introduced. Then, the radiative characteristics are experimentally determined, and analyses of chemical compositions, elements, and particle size distributions of the tested ash samples are also presented. The performance of the optical emission-based method for the measurement of the average surface temperature and surface temperature distribution is also experimentally verified. Finally, the findings of this study are summarized.

Experimental set-up

Ash samples were heated using a Hencken flat-flame burner that consists of hundreds of non-premixed flamelets. The burner was the same as that used in the work by Gao *et al.* [32], however, in the present study, the burner was placed facing upward. Flames were generated using CH_4, air, and O_2. Figure 1 schematically illustrates the details of the experimental set-up. A narrow piece of stainless steel wire mesh was placed above the burner to separate the flame from a *K*-type thermocouple, and the wire mesh did not touch the burner. The longer side of the wire mesh was longer than the burner, guaranteeing that few emissions of the flame could be detected above and along the longer side of the wire mesh. The *K*-type thermocouple was suspended above the wire mesh without touching it, and was placed along the longer side of the wire mesh. A small lump of ash sample was stacked on the front end of the thermocouple, and was protected by the wire mesh from being blown away.

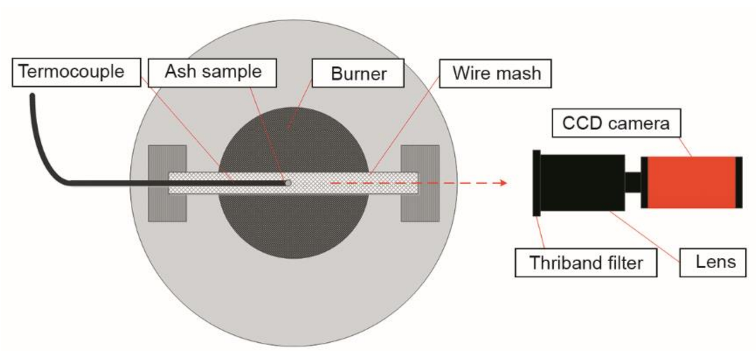

Figure 1. Experimental system

A color camera (type: Manta G504C) equipped with a lens (type: Computar TEC-M55) was used to take images along the longer side of the wire mesh. The front of the lens was equipped with a tri-band filter (type: Edmund 432, 517, and 615 nm Tri-Band Filter), the parameters of which are reported in tab. 1. Each of the three bands allowed radiation around the center wavelength to pass through one of the camera's optical channels, *i.e.*, the R, G, or B channel. The imaging system containing the camera, lens, and filter was calibrated using a blackbody furnace (type: Mikron M330). The calibrations of each optical channel established the relationship between the response value divided by the exposure time and the intensity captured by the camera. After calibration, the parameters of the lens and camera, excluding the exposure time, were fixed. Moreover, the distance between the imaging system and the ash sample was the same with that between the black body furnace and the system during cal-

Table 1. Parameters of the tri-band filter

	Band	Band	Band
Center wave-length [nm]	432	517	615
Bandwidth [nm]	36	23	61

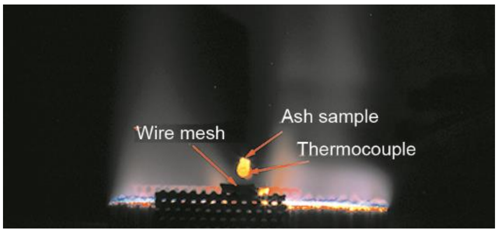

Figure 2. Image of the ash sample, thermocouple, and flame

ibration. Figure 2 is an image taken by the camera. As shown in the figure, the thermocouple and ash samples were separated from the flame. Moreover, the amount of each ash sample was very small, and the ash sample covered the upper surface of the thermocouple. Therefore, the average temperature of the ash sample was assumed to be the same as that of the head of the thermocouple.

Analysis of ash samples

Determination of radiative characteristics

Three types of ash samples, respectively collected from a pulverized coal-fired boiler (PCFB), a circulating fluidized bed boiler (CFB), and an industrial boiler (IB), were experimentally investigated. The radiation intensity of each sample was determined based on the images captured using the camera. Figure 3 presents the response values per millisecond for the R, G, and B optical channels at different temperatures, based on a series of experiments. It can be seen that the ash samples collected from the PCFB had a higher radiation capacity than the other two types. The values in the B optical channels were much smaller than those in the R and G optical channels, this is because the radiation intensity decreases as the wavelength decreases. Moreover, some differences were found between the first center wavelength of the tri-band filter (432 nm) and the wavelength with the strongest response of the B optical channel. Therefore, this paper investigates a two-color method that uses the radiation intensity at the R and G optical channels to calculate the temperature. In the calculations mentioned previously, the values were the averages of 11 × 11 pixels located inside and near the top of the ash sample area.

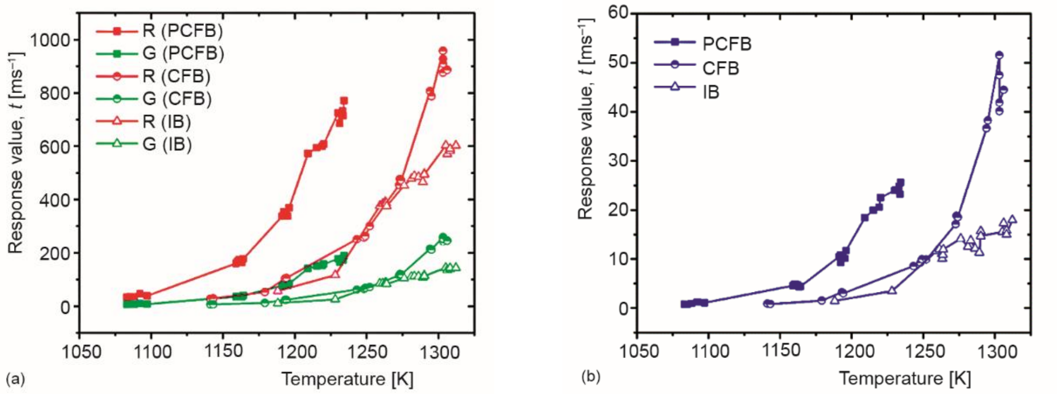

Figure 3. Response values per millisecond in (a) R and G optical channels and (b) B optical channel

According to Planck's Law, given the radiation intensity and temperature, emissivity can be calculated:

$$\varepsilon(\lambda) = \frac{I(\lambda)}{\dfrac{c_1}{\pi\lambda^5(\mathrm{e}^{c_2/\lambda T} - 1)}} \tag{1}$$

where $\varepsilon(\lambda)$ is the emissivity, c_1 and c_2 – the radiation constants, and T – the temperature. According to Wien's approximation, the temperature can be calculated using the intensity of two wavelengths:

$$T = \frac{c_2\left(\dfrac{1}{\lambda_G}-\dfrac{1}{\lambda_R}\right)}{\ln\left[\dfrac{I_R}{I_G}\dfrac{\varepsilon_G}{\varepsilon_R}\left(\dfrac{\lambda_R}{\lambda_G}\right)^5\right]} \tag{2}$$

The emissivity ratios are necessary for the two-color method, and can be determined according to the radiation intensity at known temperatures using eq. (1). Based on a series of experiments, and according to the temperatures provided by the thermocouple and the intensities given by the imaging system, the emissivity ratios at different temperatures for the three types of ash samples were experimentally determined, as presented in fig. 4. As shown in this figure, each ratio fluctuated in a range smaller than 0.1, thus establishing the implementation basis of the two-color method. Using the average ratios presented in tab. 2, the two-color method was adopted.

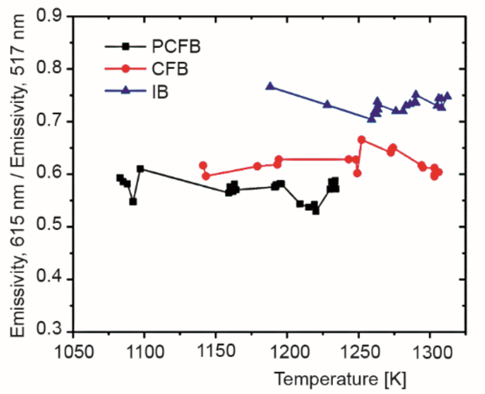

Figure 4. Emissivity ratios between 615 nm, R, and 517 nm, G

Table 2. Average ratios between emissivity at 615 nm and 517 nm

Type	PCFB	CFB	IB
Emissivity, 615 nm/Emissivity, 517 nm	0.57	0.62	0.73

Analyses of chemical compositions, elements, and particle sizes

The analyses of chemical compositions and elements were conducted using an X-ray fluorescence (XRF) analysis device (type: PANalytical B.V.-AXIOS), and the results are exhibited in fig. 5. It can be seen from the figure that the composition and elements of all three types of ash samples were similar in some respects, but different in others. The analysis of the particle sizes was conducted using a laser particle analyzer (type: Beckman Coulter LS 13 320), and the results are presented in fig. 6. As shown in the figure, the ash samples collected from the PCFB had the largest particles. Therefore, different chemical compositions, elements, and particle sizes result in different radiation capacities [33].

Results and discussion

Measurement of the average surface temperature using the two-color method

Using the average emissivity ratios of the wavelengths of the R and G optical channels presented in tab. 2, the two-color method was used to determine the average surface temperature using eq. (2). Figure 7 presents the temperature results, along with the temperatures given by the thermocouple and the relative errors. The figure indicates that, within the temperature range of the experiments, the two-color method provided temperature results with relative errors within the range of ±2%.

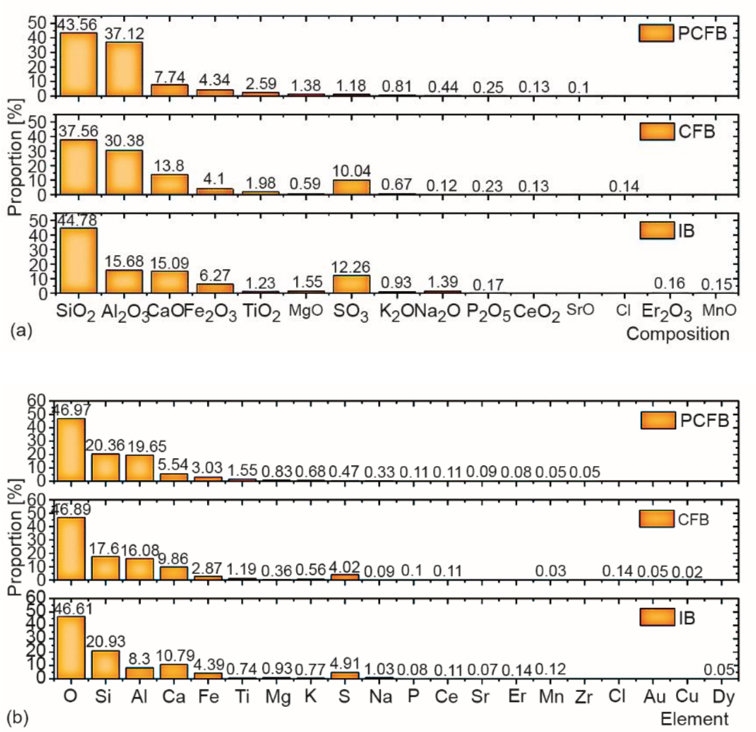

Figure 5. Results of XRF analysis; (a) chemical compositions and (b) elements

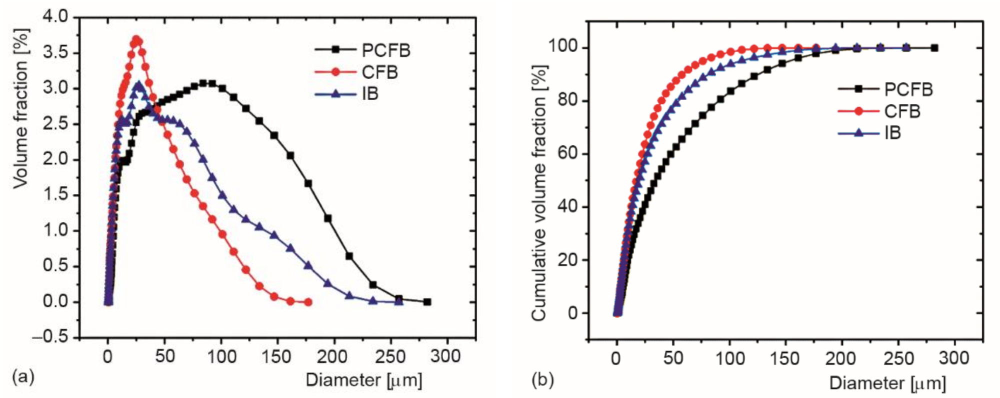

Figure 6. Particle size distributions; (a) volume fractions and (b) cumulative volume fractions

According to eq. (2), the error caused by the calculation can be estimated:

$$(\Delta T)^2 = \left(\frac{\partial T}{\partial r_{RG}}\Delta r_{RG}\right)^2 + \left(\frac{\partial T}{\partial I_R}\Delta I_R\right)^2 + \left(\frac{\partial T}{\partial I_G}\Delta I_G\right)^2 =$$

$$= \left[\frac{\lambda_R \lambda_G T^2}{c_2(\lambda_R - \lambda_G)}\frac{\Delta r_{RG}}{r_{RG}}\right]^2 + \left[\frac{\lambda_R \lambda_G T^2}{c_2(\lambda_R - \lambda_G)}\frac{\Delta I_R}{I_R}\right]^2 + \left[\frac{\lambda_R \lambda_G T^2}{c_2(\lambda_R - \lambda_G)}\frac{\Delta I_G}{I_G}\right]^2 \tag{3}$$

$$\left(\frac{\Delta T}{T}\right)^2 = \left[\frac{\lambda_R \lambda_G T}{c_2(\lambda_R - \lambda_G)}\frac{\Delta r_{RG}}{r_{RG}}\right]^2 + \left[\frac{\lambda_R \lambda_G T}{c_2(\lambda_R - \lambda_G)}\frac{\Delta I_R}{I_R}\right]^2 + \left[\frac{\lambda_R \lambda_G T}{c_2(\lambda_R - \lambda_G)}\frac{\Delta I_G}{I_G}\right]^2$$

where r_{RG} equals $\varepsilon_R/\varepsilon_G$. With the measurement noise for both two intensities at 1%, and with the relative error in the emissivity ratio of 5%, according to fig. 4, when T = 1300 K, the estimated relative error of the temperature was 1.52%. The experimental results and the uncertainty analysis demonstrate that the emission-based two-color method in the visible light region can provide reliable results of the average surface temperature of high temperature ash samples.

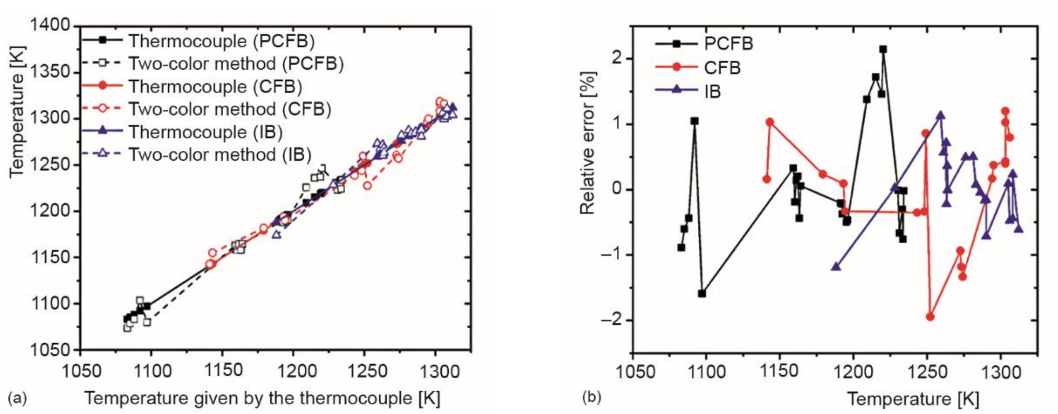

Figure 7. Surface temperatures measured using the two-color method; (a) average temperatures and (b) relative errors

Measurement of surface temperature distributions

The calculations reported in the previous subsection were conducted using average values of 11 × 11 pixels located inside and near the top of the fly ash area. The two-color method could also be used to calculate the surface temperature distribution for the entire fly ash area. Figure 8(b) shows the surface temperature distribution of fly ash collected from the PCFB when the temperature provided by the thermocouple was 960 °C, *i.e.*, 1233.15 K. Figure 8(a) indicates the calculation area. The images captured by the camera contain 2056 × 2452 pixels. Figure 9 shows the surface temperature distribution of the ash samples collected from the CFB boiler, and the temperature provided by the thermocouple was 1000 °C, *i.e.*, 1273.15 K. Here, the amount of the ash sample was less than those in the other two cases. As shown in fig. 9(b), the temperatures of the right side were closer to that provided by the thermocouple. This may be because the amount of the ash sample was greater; the other areas might have smaller ash sample and were consequently more easily influenced by disturbances in the experiments. For ash samples collected from the CFB boiler and the IB, the emissions were weaker than those of the ash sample collected from the PCFB. Moreover, the thermocouple also emits radiation at high temperatures. Therefore, in the measurements of the ash samples collected from the CFB boiler and the IB, the front end of the wire mesh was folded up to shelter the emissions of the thermocouple, thus making the thermocouple unrecognized in the images. Figure 10 presents the surface temperature distribution of ash samples collected from the IB when the thermocouple read 990 °C, which equates to 1263.15 K. The results demonstrate that the emission-based two-color method can provide reliable surface temperature distributions for high-temperature ash samples.

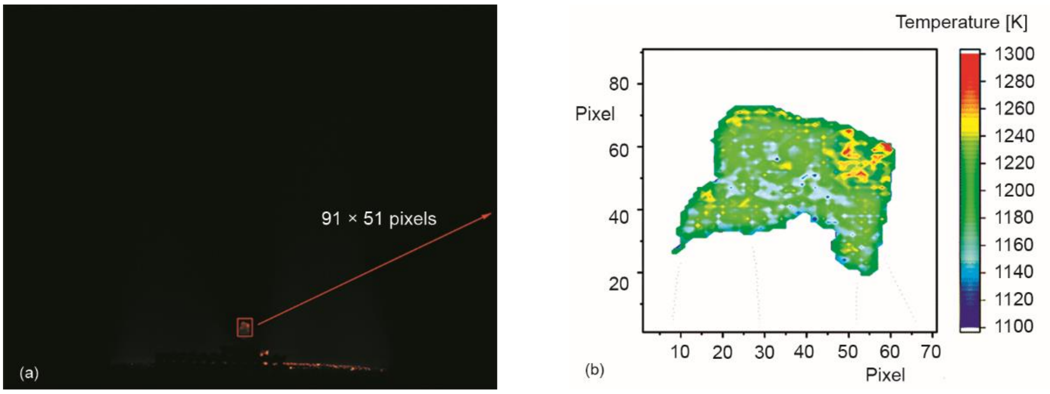

Figure 8. Surface temperature distribution of the ash sample collected from the PCFB, 1233.15 K; (a) image (exposure time = 60 ms) and (b) temperature distribution

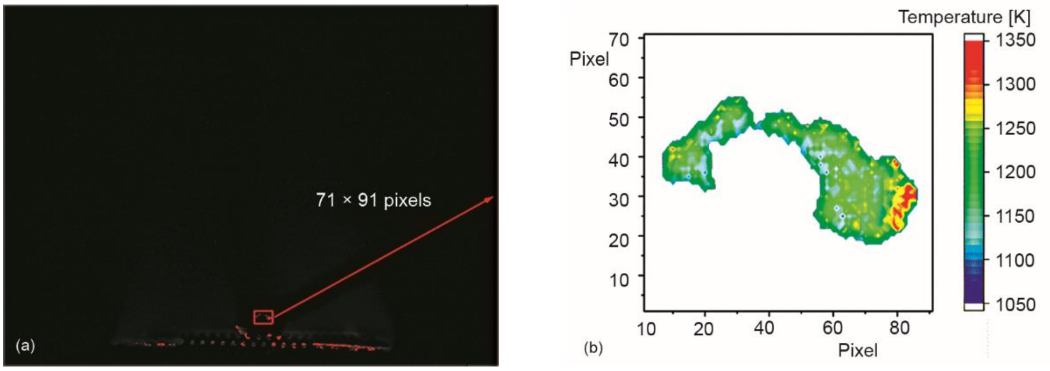

Figure 9. Surface temperature distribution of the ash sample collected from theCFB boiler 1273.15 K; (a) image (exposure time = 60 ms) and (b) temperature distribution

Lower limit of the temperature measurement using the two-color method

Ash samples with temperatures lower than those presented in figs. 3, 4, and 7, were also experimentally investigated using the two-color method. Figure 11 presents an image of the ash sample collected from the PCFB at a temperature of 680 °C, *i.e.*, 953.15 K. The other parts of the thermocouple can be recognized, as indicated by the arrow on the right side of the figure. The experiments were conducted in a dark room, demonstrating that the emission of the ash sample was very weak. Moreover, the exposure time of the image

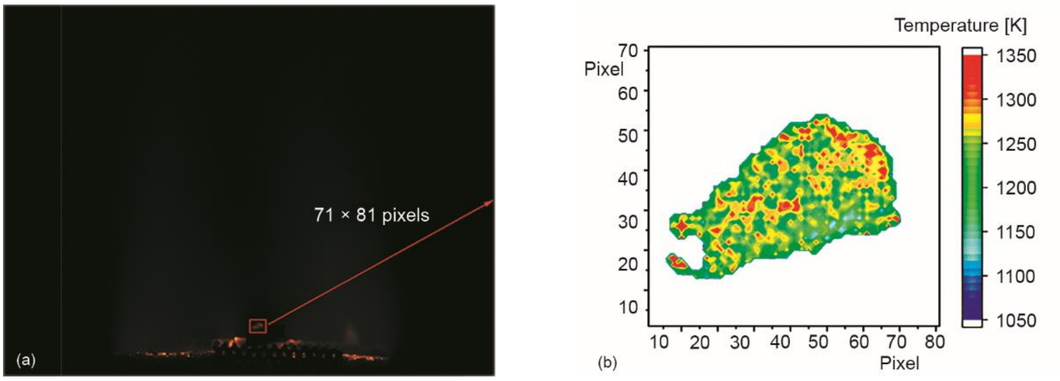

Figure 10. Surface temperature distribution of the ash samples collected from the IB, 1263.15 K; (a) image (exposure time = 60 ms) and (b) temperature distribution

was 10 seconds, which is not suitable for real-time measurement. Therefore, in this situation, the results of the method are not reliable. In other words, the emission-based two-color method in the visible light region has a lower limit when measuring temperature. Table 3 reports the average surface temperatures and relative errors at lower temperatures, which also resulted in lower response values per millisecond. Moreover, the parameters of the lens were fixed to be consistent with those used during the calibrations. Therefore, the response values per millisecond can be improved with larger apertures to receive more light and a higher radiation capacity of the ash samples to be studied, resulting in more reliable results at lower temperatures, thereby reducing the lower limit of the measurable temperature scope.

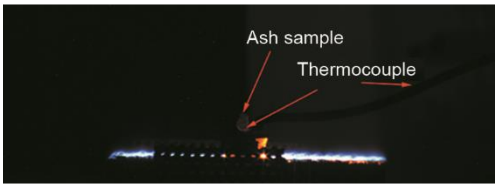

Figure 11. Image with low temperature (ash sample collected from the PCFB, temperature = 953.15 K, exposure time = 10000 ms)

Table 3. Measurement results at low temperatures

Type	Temperature [K]	R/t [ms^{-1}]	G/t [ms^{-1}]	Measured temperature [K]	Relative error [%]
PCFB	953.15	1.03	0.21	3787.92	297.41
	1022.15	8.91	1.70	566.78	–44.55
CFB	1093.15	10.06	2.31	924.22	–15.45
	1103.15	12.05	3.49	1121.75	1.69
	1116.15	13.18	4.64	1244.20	11.47
IB	1117.15	10.41	1.97	819.11	–26.68
	1123.15	8.94	1.68	499.45	–55.53
	1154.65	24.91	4.84	1100.48	–4.69
	1163.15	14.78	2.75	976.85	–16.02
	1185.15	44.15	8.58	1152.59	–2.75

Conclusion

Three types of fly ash samples respectively collected from a PCFB, a CFB, and an IB were experimentally investigated. A Hencken flat-flame burner was used to heat the ash samples to high temperatures, and a color camera equipped with a tri-band filter was used to capture radiation images. The radiative characteristics were determined based on a series of experiments using the temperatures recorded by a thermocouple and intensities given by the imaging system. Analyses of the chemical compositions, elements, and particle sizes were also provided. An emission-based two-color method for use in the visible light region was experimentally analyzed and verified, and an uncertainty analysis was provided. The conclusions of the work are summarized as follows.

- The use of the emission-based two-color method in the visible light region can provide reliable results of average surface temperatures when the radiation emitted from the ash samples is obviously larger than the ambient light.
- The method can also provide reliable surface temperature distributions for high-temperature ash samples.
- The method has a lower limit of temperature measurement, which can be lessened with larger apertures to receive more light and a higher capacity of the ash samples to be studied.

Acknowledgement

This research was supported by the National Natural Science Foundation of China (No. 51827808), *Thirteenth Five-Year* National Key R&D Program of China (2018YFC1903000), the China Energy Science and Technology Project (No. GJNY-18-27), and the Fundamental Research Funds for the Central Universities (No. 2018ZD03).

The authors also acknowledged the discussion with Prof. Yiyang Zhang and Dr. Ye Yuan.

Nomenclature

c_1 – radiation constant [Wm^3]
c_2 – radiation constant [mK]
I – radiation intensity [Wm^{-3}Sr^{-1}]
T – temperature [K]

Greek symbols

ε – emissivity [–]
λ – wavelength [m]

References

[1] Huang, L. Y., *et al.*, Prediction of Ash Deposition on suPerheater Tubes from Pulverized Coal Combustion, *Fuel*, *75* (1996), 3, pp. 271-279
[2] Tang, S., *et al.*, Fouling Characteristics Analysis and Morphology Prediction of Heat Exchangers with a Particulate Fouling Model Considering Deposition and Removal Mechanisms, *Fuel*, *203* (2017), Sept., pp. 725-738
[3] Huang, Q., *et al.*, Numerical and Experimental Study on the Deposition of Fine Particulate Matter During the Combustion of Pulverized Lignite Coal in a 25kW Combustor, *Powder Technology*, *317* (2017), July, pp. 449-457
[4] Cai, Y., *et al.*, Modeling of Ash Formation and Deposition Processes in Coal and Biomass Fired Boilers: A Comprehensive Review, *Applied Energy*, *230* (2018), Nov., pp. 1447-1544
[5] Zhou, H., *et al.*, Investigation of the Deposition Characteristics of Ammonium Bisulfate and Fly Ash Blend Using an On-Line Digital Image Technique: Effect of Deposition Surface Temperature, *Fuel Processing Technology*, *179* (2018), Oct., pp. 359-368
[6] Zhang, J., *et al.*, Experimental Study on the Ash Deposit Thermal Conductivity for Ammonium Bisulfate and Fly Ash Blend with an in Situ Measurement Technology, *Fuel*, *263* (2020), Mar., pp. 116575

[7] Yang, X., *et al.*, Understanding the ash Deposition Formation in Zhundong Lignite Combustion Through Dynamic CFD Modelling Analysis, *Fuel*, *194* (2017), Apr., pp. 533-543
[8] Wang, Y., *et al.*, Understanding Ash Deposition for Zhundong Coal Combustion in 330MW Utility Boiler: Focusing on Surface Temperature Effects, *Fuel*, *216* (2018), Mar., pp. 697-706
[9] Kupka, T., *et al.*, Effect of Fuel Type and Deposition Surface Temperature on the Growth and Structure of an Ash Deposit Collected During Cofiring of Coal with Sewage Sludge and Sawdust, *Energy & Fuels*, *23* (2009), 7, pp. 3429-3436
[10] Laxminarayan, Y., *et al.*, Biomass Fly Ash Deposition in an Entrained Flow Reactor, *Proceedings of the Combustion Institute*, *37* (2019), 3, pp. 2689-2696
[11] Zhou H., *et al.*, Investigation of Slagging Characteristics in a 300 kW Test Furnace: Effect of Deposition Surface Temperature, *Industrial & Engineering Chemistry Research*, *53* (2014), 17, pp. 7233-7246
[12] Mu, L., *et al.*, Unsteady CFD Simulation on Ash Particle Deposition and Removal Characteristics in Tube Banks: Focusing on Particle Diameter, Flow Velocity, and Temperature, *Journal of the Energy Institute*, (2020)
[13] Zhimin, Z., *et al.*, A Novel Method Used to Study Growth of Ash Deposition and in Situ Measurement of Effective Thermal Conductivity of Ash Deposit, *Heat Transfer Research*, *47* (2018), 2, pp. 271-285
[14] Panchal, S., *et al.*, Thermal Modeling and Validation of temperature Distributions in a Prismatic Lithium-Ion Battery at Different Discharge Rates and Varying Boundary Conditions, *Applied Thermal Engineering*, *96* (2016), Mar., pp. 190-199
[15] Nascimento, M., *et al.*, Real Time Thermal Monitoring of Lithium Batteries with fiber Sensors and Thermocouples: A Comparative Study, *Measurement*, *111* (2017), Dec., pp. 260-263
[16] Gomes, M. J., *et al.*, Experimental Study on Combined Buoyant-Thermocapillary Flow Along with Rising Liquid Film on the Surface of a Horizontal Metallic Mesh Tube, *Frontiers in Energy*, *14* (2017), July, pp. 1-13
[17] Martinez, D., *et al.*, Embedded Thermocouple Wall Temperature Measurement Technique for Scraped Surface Heat Exchangers, *Applied Thermal Engineering*, *114* (2017), Mar., pp. 793-801
[18] Salinero, J., *et al.*, The Effect of Using Thermocouples on the Char Particle Combustion in a Fluidized Bed Reactor, *Fuel*, *207* (2017), Nov., pp. 615-624
[19] Zhu, M., *et al.*, Ignition of Single Coal Particle in a Hot Furnace Under Normal- and Micro-Gravity Condition, *Proceedings of the Combustion Institute*, *32* (2009), 2, pp. 2029-2035
[20] Liu, H., *et al.*, Measurement of Distributions of Temperature and Wavelength-Dependent Emissivity of a Laminar Diffusion Flame Using Hyper-Spectral Imaging Technique, *Measurement Science and Technology*, *27* (2015), 2, 025201
[21] Lukovic, M., *et al.*, Two-Color Pyrometer-Based Method for Measuring Temperature Profiles and Attenuation Coefficients in a Coal Power Plant, *Combustion Science and Technology*, *190* (2018), 11, pp. 2018-2029
[22] Liu, H., *et al.*, Experimental Study of Radiation Characteristics and Temperature Distributions of Gasoline and Biomass Flame, *IET Renewable Power Generation*, *13* (2019), 11, pp. 1833-1839
[23] Liu, H., *et al.*, Measurement of Temperature and Wavelength-Dependent Emissivity Distributions Using Multi-Wavelength Radiation Thermometry, *Optics Communications*, *472* (2020), Oct., ID 125895
[24] Zhao, H., *et al.*, Optical Diagnostics for Soot and Temperature Measurement in Diesel Engines, *Prog. Energy. Combust. Sci.*, *24* (1998), 3, pp. 221-255
[25] Ma, B., *et al.*, Intensity-Ratio and Color-Ratio Thin-Filament Pyrometry: Uncertainties and Accuracy, *Combustion and Flame*, *161* (2014), 4, pp. 908-916
[26] Yao, X., *et al.*, High Throughput Dual-Wavelength Temperature Distribution Imaging Via Compressive Imaging, *Optics Communications*, *410* (2018), Mar., pp. 287-291
[27] Huang, Y., *et al.*, Quantifying the Effects of Combustion Gases' Radiation on Surface Temperature Measurements Using Two-Color Pyrometry, *Energy & Fuels*, *33* (2019), 4, pp. 3610-3619
[28] Huang, Q., *et al.*, In Situ Diagnostics on the Dynamic Processes of Ash Deposit Formation, Shedding, and Heat Transfer in a Self-Sustained Down-Fired Furnace, *Energy & Fuels*, *32* (2018), 4, pp. 4424-4431
[29] Xu, Y., *et al.*, Measurement on the Surface Temperature of Dispersed Chars in a Flat-Flame Burner Using Modified RGB Pyrometry, *Energy & Fuels*, *31* (2017), 3, pp. 2228-2235
[30] Yan, W., *et al.*, Experiments Investigation on 2D Distribution of Soot Temperature and Volume Fraction by Image Processing of Visible Radiation, *Applied Thermal Engineering*, *124* (2017), Sept., pp. 1014-1022

[31] Mason, P. E., *et al.,* Observations on the Release of Gas-Phase Potassium During the Combustion of Single Particles of Biomass, *Fuel*, *182* (2016), Oct., pp. 110-117
[32] Gao, Q., *et al.,* Ultrafine Particulate Matter Formation in the Early Stage of Pulverized Coal Combustion of High-Sodium Lignite, *Fuel*, *158* (2015), Oct., pp. 224-231
[33] Greffrath, F., *et al.,* Influence of Chemical Composition and Physical Structure on Normal Radiant Emittance Characteristics of Ash Deposits, *Fuel*, *134* (2014), Oct., pp. 307-314

Paper submitted: June 20, 2020
Paper revised: May 10, 2021
Paper accepted: May 16, 2021